Proceedings of the 5th International Marine Design Conference
May 24-27, 1994, Delft, the Netherlands

Optimal Design of Thruster System for Superconducting Electromagnetic Propulsion Ship

Shinsuke AKAGI, Kikuo FUJITA and Kazuo SOGA

Department of Mechanical Engineering for Industrial Machinery and Systems
Faculty of Engineering
Osaka University
JAPAN

Mailing Address: Professor Shinsuke Akagi, Department of Mechanical Engineering for Industrial Machinery and Systems, Faculty of Engineering, Osaka University, 2-1 Yamadaoka, Suita, Osaka 565, JAPAN

ABSTRACT

Optimal design of magnetohydrodynamic (MHD) thruster systems for a superconducting electromagnetic propulsion ship is presented. Optimal designs of the configurations of thrusters are searched for three kinds of thruster systems, namely, the inner ducting, the annular ducting and the pod mount type which are designed to install an experimental ship with SWATH hulls. After that, the optimal design maximizing the propulsive efficiency is examined and evaluated. The results show that the inner ducting type is of the highest propulsive efficiency, while the annular type is lowest. And the pod mount type is ranked between these two. In general, however, efficiency of a MHD thruster system is very low compared with conventional propulsion systems. In order to improve the efficiency, level-up of superconducting technology including new-material is urged.

1 Introduction

The magnetohydrodynamic (MHD) thruster system for ships with superconducting electromagnets has been recognized as its potentially attractive performance. Namely, it does not need any rotating part like conventional propellers or waterjet propulsions, and therefore may be less affected by cavitation, which would be suitable propulsion means for high speed ships and for ships as specially required silent operation. However, it is still considered that the MHD thruster system has various kind of difficult problems to be resolved before it could reach the level of practical use.

The problems may be classified into two categories, which are the technology specifically concerning physical phenomena of superconductors and practical technique which examines possibility for designing and constructing MHD thruster systems. This investigation concerns with the later kind of problems.

It is considered that MHD thrusters can be designed with freedom for determining their configurations and size so that they could have high propulsive performance because shaftings are not required. Some possible configurations of MHD thruster systems have been proposed for ship propulsion [DORAGH 1963] [WAY 1967] [SWALLOM 1991] [MOTORA 1991]. However, advantage and disadvantage among them have not been discussed, and it has not also been ascertained which configuration of the system is the optimal one.

In this feasibility study, optimal designs of the configurations for MHD thrusters are searched with maximizing the propulsive efficiency among three kinds of thruster systems for an experimental ship. Namely, the inner ducting, the annular ducting and the pod mount type are designed for installation respectively to a SWATH hull. After that, each optimal design is examined and evaluated.

2 A MHD Ship and its Thruster Systems

A MHD ship has novel type thrusters which generate thrust force conducted by electromagnetic force (Fig. 1). Force (Lorentz force) is created in sea water by means

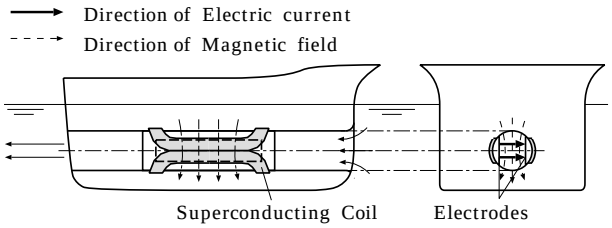

Fig. 1 Principle of the MHD thruster

of electromagnets and electrodes installed inside or outside a ship. Studies on the MHD ship have continued since a patent applied by W. A. Rice in 1961 [RICE 1961]. Although its principle is simple, very strong electromagnetic force is necessary to gain effective thrust force because the electrical conductivity of sea water is very low.

In the early 1960s, L. R. A. Doragh proposed to apply superconducting magnets to overcome this difficulty [DORAGH 1963]. After then, numerous studies have been continued for investigating how to apply it to the ship's thruster system. For example, just after Doragh, S. Way designed an experimental ship with the length of 3.1 m and tried the running test [WAY 1967].

Recently, a full scale experimental MHD ship "YAMATO-1" was built and the study was conducted to investigate feasibility for applying the MHD thruster system to actual ships [MOTORA 1991], which would be motivated by the successful application of superconducting magnets to the MAGLEV (Magnetic levitating) test train.

Concerning the application of the MHD propulsion to a ship, two kinds of basic configurations have been proposed to realize the superconducting thruster as the ship's propulsion system. One is the outer magnet field system, and the other is the inner magnet field system. In the case of the later system, superconducting magnets are installed inside a ship's hull, which is suitable for shielding MHD field against surroundings. In this study, the inner magnet field system will be treated.

Figure 1 illustrates the basic principle of the inner magnet thruster system. In this system, superconducting coils cooled with liquid helium and electrodes installed in a ship's hull form a electromagnetic field, in which sea water is led and accelerated by MHD force and generate thrust. Although this system is suitable for shielding the electromagnetic field as mentioned above, the flow resistance in a duct is slightly high, and its performance is very much influenced by the configuration and the shape of the thruster duct etc. Therefore, the optimization procedure

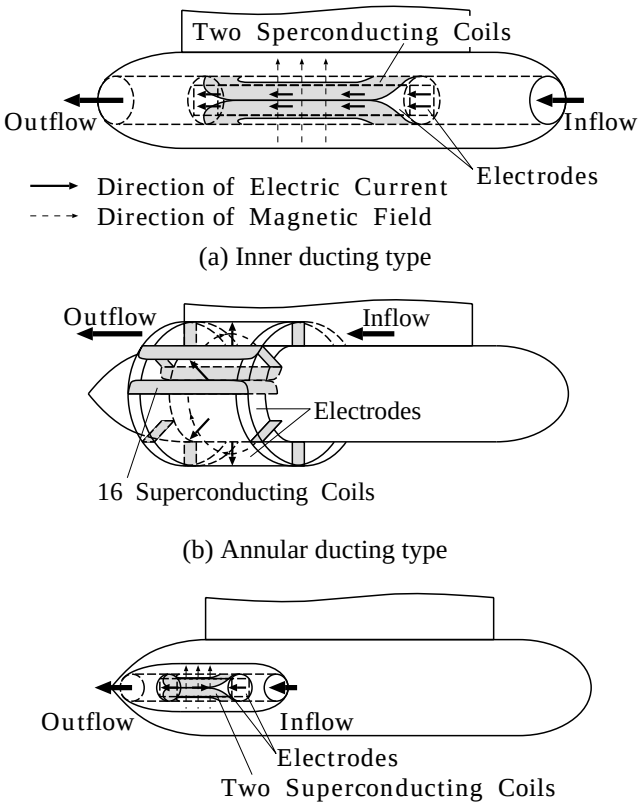

(a) Inner ducting type

(b) Annular ducting type

(c) Pod mount type

Fig. 2 Three types of MHD thruster systems

is required to determine them so that they have a well balanced performance.

As a basic hull form for this study, a SWATH type ship was selected (Fig. 3), which would be suitable for the installation of MHD thrusters, and also has flexibility for the configuration design of thruster systems. The configurations of thruster systems were selected as the following three types as shown in Fig. 2.

Inner ducting type (Fig. 2 (a)) — A thruster duct is installed in the lower hull of a SWATH, which accelerates sea water for generating thrust force. Two saddle type superconducting coils and electrodes installed in the duct generate electromagnetic fields as shown in Fig. 2 (a).

Annular ducting type (Fig. 2 (b)) — Superconducting magnets are composed of several segments which are installed surrounding the lower hull of a SWATH [SWALLOM 1991]. The magnets and electrodes form an annular ducting surrounding the lower hull, which generates electromagnetic fields as shown in Fig. 2 (b).

Pod mount type (Fig. 2 (c)) — Two pods of thrusters are

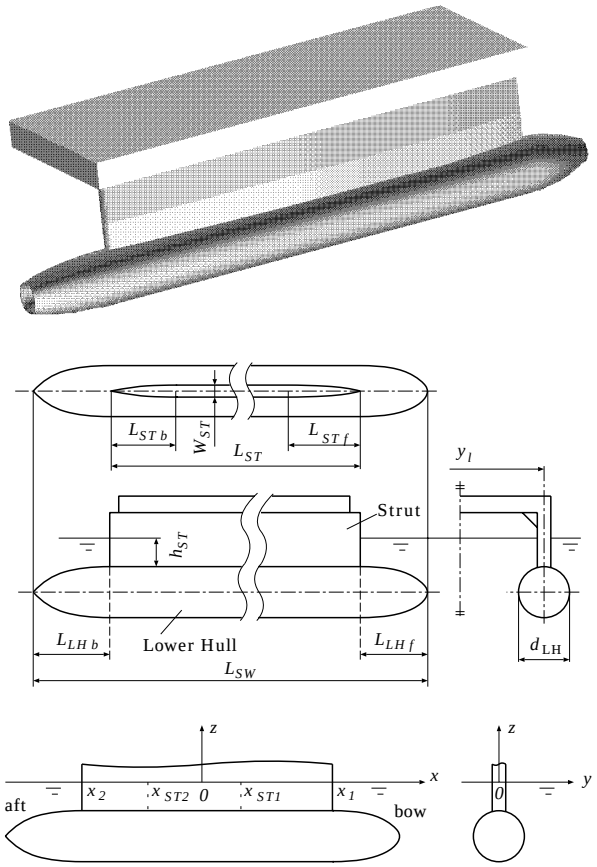

Fig. 3 SWATH type hull configuration and its coordinate system

installed at both sides of the lower hull of a SWATH type ship. Their configuration is similar to a inner ducting type thruster as shown in Fig. 2 (c).

3 Modeling of the MHD Thruster Systems and Performance Calculations

Before discussing the optimization, modeling of MHD thruster systems and their performance calculations are mentioned briefly.

3.1 Hull form definition of a SWATH type ship and the formula of its resistance

Figure 3 illustrates a SWATH type configuration which will be adopted in the following calculations. Each point of the hull surface is defined by the coordinate system as shown in Fig. 3. The shape of the surface is defined as a spheroidal form in the forepart and as a parabolic-revolution form in the aftpart, together with a parallel form in the midpart.

The total resistance, R_T of the SWATH ship is calculated as the sum of three components [SALVESEN 1985] [PAPANIKOLAOU 1991],

$$R_T = R_W + R_F + R_{APP} \tag{1}$$

where, R_W : wave making resistance of the bare hull, R_F: frictional resistance of the bare hull, R_{APP} : appendage resistance. Each of three components is calculated by a simplified theory as discussed below.

Wave-making resistance R_W The formula for wave-making resistance of the ship is taken referring to Chapman. The ship holds a twin hull with a distance y_l apart, moving in a deep canal of width W_{ch} [CHAPMAN 1972].

$$R_W = \frac{16\pi^2\rho K_0}{W_{ch}} \left\{ ({I_{SW_0}}^2 + {J_{SW_0}}^2) + 2\sum_{n=1}^{\infty} ({I_{SW_n}}^2 + {J_{SW_n}}^2) \frac{\cosh^2(u_m)}{\sinh(2u_n)} \right\} \tag{2}$$

$$\begin{aligned} I_{SW_n} + iJ_{SW_n} &= I_{SW}(u_n) + iJ_{SW}(u_n) \\ &= \sum_l \cos\{K_0 \frac{y_l}{2} \sinh(2u_n)\} \\ &\quad \times \{I_l(u_n) + iJ_l(u_n)\} exp(imx_l) \end{aligned} \tag{3}$$

$$\begin{aligned} I_l(u_n) + iJ_l(u_n) &= -\frac{U}{2\pi} \int\int \frac{\partial \eta}{\partial x} exp(imx + zm^2K_0^{-1}) dxdz \end{aligned} \tag{4}$$

where, ρ : sea water density, $K_0 = g/U^2$, $\sinh(2u_n) = 4\pi n/K_0 W_{ch}$, $m = K_0 \cosh(u_n)$, g : gravitational constant, U: ship's velocity, $(I_l + iJ_l)$: components of wave-making resistance when the hull form component l moving independently, x, y, z : the coordinates fixed to the hull form component, x_l, y_l : the coordinates of the origin of the hull form component l against the ship.

In the calculation of equation (2), the value of W_{ch} must be selected so that $K_0 W_{ch} \gg 1$ is satisfied. The definition of η in equation (4) represents the projection of the hull surface, which can be written as $y = \pm\eta(x,z)$.

The wave-making resistance of each respective component l of hull forms can be calculated by equation (4).

(1) Lower hull part The submerged lower hull is assumed to be an axisymmetrical slender form. Thus, the integral in equation (4) can be approximated as

$$\begin{aligned} \int \frac{\partial \eta}{\partial x} exp(zm^2K_0^{-1}) dz &= exp(-fm^2K_0^{-1}) \int \frac{\partial \eta}{\partial x} dz \\ &= \frac{1}{2} exp(-fm^2K_0^{-1}) \frac{dA}{dx} \end{aligned} \tag{5}$$

where, $A = A(x)$ represents the sectional area of the hull at x in Fig. 3. The above integral is calculated based on the function $A(x)$ in Fig. 3.

(2) Strut The parallel part at the middle of the strut does not affect on wave-making resistance. The resistance of the fore and aftpart can be calculated using equation (4) based on the function of η defined by the configuration shown in Fig. 3.

(3) Thruster The annular ducting type thruster and the pod mount type thruster have their own resistance. The wave-making resistance for each case can be calculated using equation (4) based on the function of η defined by the respective thruster configurations shown later in Figs. 9 and 11.

Frictional resistance R_F The bare-hull frictional resistance R_F is calculated by dividing it into three parts.

$$R_F = 2(R_{FH} + R_{FS} + R_{COR}) \tag{6}$$

where, R_{FH} : frictional resistance of the lower hull, R_{FS}: frictional resistance of the strut, R_{COR} : correlation resistance. These components of resistance are calculated by the following equations.

$$R_{FH} = \frac{1}{2} F_{FH} \rho U^2 C_{FH} A_H \tag{7}$$

$$R_{FS} = \frac{1}{2} F_{FS} \rho U^2 C_{FS} A_S \tag{8}$$

$$R_{COR} = \frac{1}{2} \rho U^2 C_A (A_S + A_H) \tag{9}$$

where, F_{FH} : the form factor of the hull (= 1.10), F_{FS} : the form factor of the strut (= 1.17), C_{FH}, C_{FS} : the frictional resistance coefficients of the hull and the strut respectively, C_A: the correlation resistance coefficient (= 0.0005), A_H, A_S : the wetted surface area for the hull and the strut respectively. The frictional resistance coefficients in equations (7), (8) and (9) are given by the following 1957 ITTC formula, namely

$$C_F = 0.057(\log_{10} Re - 2)^{-2} \tag{10}$$

where, Re : Reynolds number.

Appendage resistance R_{APP} The resistance for each appendage is estimated with the sum of the hull-appendage interference drag R_{HA} and the tip drag of the strut R_{TI}, namely

$$R_{APP} = 2(R_{AH} + R_{TI}) \tag{11}$$

R_{HA} and R_{TI} can be estimated with

$$R_{HA} = \left\{ 0.75 \left(\frac{W_{ST}}{L_{ch}} \right)^3 - 0.3 \times 10^{-3} \right\} \cdot \frac{1}{2} \rho {L_{ch}}^2 U^2$$

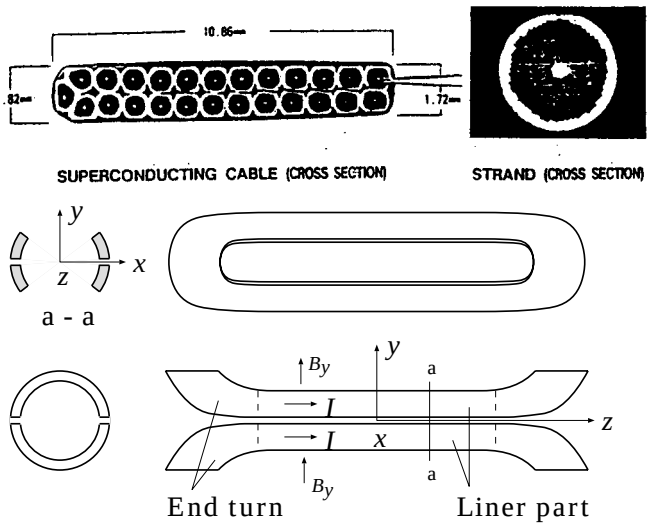

Fig. 4 Superconducting wire and coils (SHIMAMOTO et al.)

$$R_{TI} = 0.075 {W_{ST}}^2 \cdot \frac{1}{2} \rho U^2$$

where, L_{ch} : cord length of the strut, W_{ST} : width of the strut.

Furthermore, the viscous resistance of thrusters must be account additionally for the case of the annular ducting system and the pod mount system, while the case of the inner ducting system may not. These resistance can be estimated with the similar treatment as given by equation (6) for the hull frictional resistance.

3.2 Hydraulic headloss of the thruster ducts

The hydraulic headloss of the thruster ducts ΔH is estimated by calculating the frictional headloss of the ducts, the headloss of the inner and outer part of the thruster ducts, and the headloss of the diffuser nozzle of the thruster duct, which calculations are based on the well-known formula of hydraulics.

3.3 Electromagnetic field quantities

The distribution of the electromagnetic field quantities inside the MHD channel can be estimated by the following manner.

The superconducting electric coils are composed of NbTi wires as shown by Fig. 4. This design is based on the coil construction applied for the experimental ship YAMATO-1 [SHIMAMOTO 1991]. The configuration of this coil consists of a pair of the saddle type coils which generate one-directional magnetic field. The parallel part of the coils contributes mainly the uniform strength of

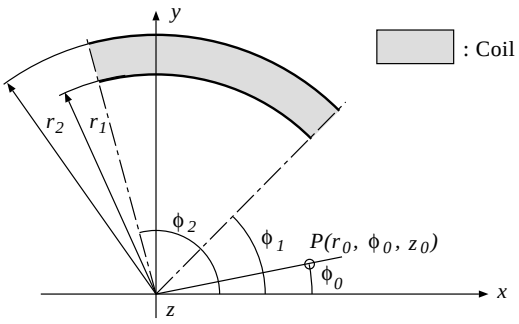

Fig. 5 Coil section

the magnetic field, which strength is estimated by the following calculation.

In the calculation, the coordinate system is taken as Fig. 5, and the magnetic field is calculated by the Biot-Savert formula for a radial section of the coil, where density of electric current is assumed to be uniform. Namely, the density of magnetic field at the point $P(r_0, \phi_0, z_0)$ is given by,

$$\left.\begin{aligned} B_r &= -\frac{\mu_0 J_{cl}}{4\pi}\int_{\psi_1}^{\psi_2}\int_{r_1}^{r_2}\left[F_R(r,\psi,z)\right]_{z_1}^{z_2} d\psi dr \\ B_\phi &= -\frac{\mu_0 J_{cl}}{4\pi}\int_{\psi_1}^{\psi_2}\int_{r_1}^{r_2}\left[F_\phi(r,\psi,z)\right]_{z_1}^{z_2} d\psi dr \end{aligned}\right\} \quad (12)$$

where, B_r, B_ϕ : density of magnetic field for r, ϕ directions, respectively. The functions F_R and F_ϕ in equation (12) are given by,

$$\left.\begin{aligned} F_R(r,\psi,z) &= \frac{zr^2\sin\psi}{G(r,\psi)\sqrt{Z^2+G(r,\psi)}} \\ F_\phi(r,\psi,z) &= \frac{z(r_0 r - r^2\cos\psi)}{G(r,\psi)\sqrt{Z^2+G(r,\psi)}} \\ G(r,\psi) &= r^2 - 2rr_0\cos\psi + r_0^2 \\ \psi &= \phi - \phi_0 \\ Z &= z_0 - z \end{aligned}\right\} \quad (13)$$

In equation (12), μ_0 denotes permeability of free space. Figure 6 illustrates an example of the calculated magnetic field for an inner ducting thruster. For the MHD thruster system, the electrodes are placed with an adequate distance in the above magnetic field so that the Lorentz force is generated for the required thrust. The calculation of the Lorentz force will be given in the next section.

In addition to the above thrust force, the superconducting coil produces the force which expands the coil itself. In order to withstand the force, it is required to install the ring type holding devices for coils (The coil support shown in Fig. 8). Their weight is also included into the total weight of the ship in the optimization calculation.

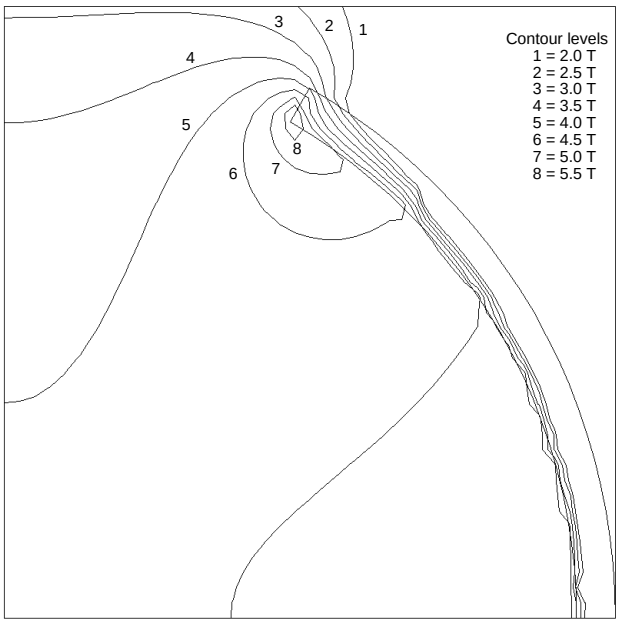

Fig. 6 Magnetic field of inner ducting thruster

3.4 The MHD force and propulsive efficiency

Based on the abovementioned calculations, the overall propulsive efficiency η_T of the ship is calculated by the following expression.

$$\eta_T = \eta_H \cdot \eta_E \quad (14)$$

where, η_H : hydraulic efficiency, η_E : electrical efficiency. The hydraulic efficiency η_H is the usual water-jet efficiency of the thruster, and the electrical efficiency is determined based on the electric power supplied. Namely,

$$\eta_H = \frac{Thrust\ power}{Hydraulic\ power} = \frac{TU}{\rho gHQ} \quad (15)$$

$$\eta_E = \frac{Hydraulic\ power}{Electric\ power} = \frac{\rho gHQ}{P_e} \quad (16)$$

where, T : thrust, H : pumping head of the thruster, Q : flow rate in the duct, P_e : electric power.

The calculating methods for η_H, η_E and η_T are as follows.

The thrust force T at the ship's speed U is given by

$$T \approx \rho Q(W - U) \quad (17)$$

where, W : outlet flow velocity of the thruster.

In equation (17), the unknown flow velocity W can be calculated, together with η_H of equation (15), as follows. When the ship speed U is given, the resistance of the ship R_T is calculated using equation (1). The resistance R_T must

be balanced with the thrust force T given by equation (17), namely

$$\begin{aligned} R_T &= T \approx \rho Q(W-U) \\ W &\approx U + \frac{R_T}{\rho Q} \end{aligned}$$

The flow rate Q can be determined using the inlet form of the duct. Using the value W, the duct configuration and size is calculated. After that, the headloss of the thruster ΔH can be estimated as mentioned in section 3.2. The required head H in equation (15) must balance with the headloss ΔH. Thus, the hydraulic efficiency η_H of equation (15) can be then determined. These procedure are repeated in the optimization calculation, which will be explained in the later section.

On the other hand, the electric efficiency η_E can be calculated as follows. The density of magnetic field B is given by equation (12) as mentioned in section 3.3. Using the value B, the MHD force f acting on the unit volume of sea water in the duct can be given by the Lorentz formula, as follows.

$$f = j \times B \tag{18}$$

where, j : electric current density in the unit volume of sea water.

The current density j can be given by,

$$j = \sigma(E + v \times B) \tag{19}$$

where, E : electric field, v : velocity of sea water in the duct, σ : electrical conductivity of sea water(= 4.0 [1/Ω m]). Equations (18) and (19) can be written with a scalar expression for the thruster ducting, as follows.

$$f = J \cdot B \tag{20}$$

$$J = \sigma\left(\frac{dV}{dL} - U_w \cdot B\right) \tag{21}$$

where, f : MHD force acting on the unit volume of sea water in the duct, J : current density in the duct, B : density of the magnetic field in the duct, dV/dL : tangent of voltage in the duct, U_w : flow velocity in the duct.

If the density of J and B is uniform in the duct, equations (20) and (21) can be integrated as

$$F = J_e \cdot B \cdot b \tag{22}$$

$$J = \sigma\left(\frac{V_e}{b} - U_w \cdot B\right) \tag{23}$$

where, F : force acting on sea water in the duct, J_e : current in the duct ($= J \cdot a \cdot l_W$), a : width of the electrode, l_W : length of the electrode, V_e : voltage between the electrodes.

From equation (22), the pumping head of the thruster H is given by

$$H = \frac{F}{A_w \rho g} \tag{24}$$

where, A_w : sectional area of the duct.

The electric power required for propulsion is given by

$$P_e = J_e \cdot V_e \tag{25}$$

Therefore, the efficiency η_E of equation (16) can be written using equations (22), (23) and (24),

$$\eta_E = \frac{\rho g H Q}{P_e} = \frac{1}{\dfrac{J}{\sigma U_w B} + 1} \tag{26}$$

In the optimization calculation, equations (14)$\sim$ (26) relate to each other, together with the hydrodynamic and electromagnetic calculations mentioned in section 3.1 $\sim$ 3.3.

According to equation (26), it is recognized that the magnetic density B must be higher in order to improve the efficiency η_E, because the electrical conductivity σ of sea water is very low. Therefore, the superconducting electromagnet is indispensable for MHD thruster systems.

4 Optimization Procedure of the MHD Thruster System Design

4.1 Outline of the optimal design

Optimization calculation for designing the MHD thruster system is formulated individually for each type of the thruster systems; namely, the inner ducting, the annular ducting and the pod mount type thrusters. The formulation of the optimization is based on the modeling of the performance of each thruster discussed in the previous chapter. The objective function is taken as maximizing its propulsive efficiency. The design variables are selected from the geometrical dimensions of thrusters and a SWATH hull, which are determined so that the objective function is maximized under the various constraints. The constraints are formulated considering the hydraulic and the electromagnetic performance as well as the geometrical relations of the hull and the thrusters. After the optimal designs are determined for each individual system, they are compared and evaluated with each other.

Before the optimization, some design conditions are assumed to be common to the above three types of thruster systems. The ship's hull forms have a similar shape of the SWATH with the same displacement. The ship's speeds are also assumed to be identical for each case.

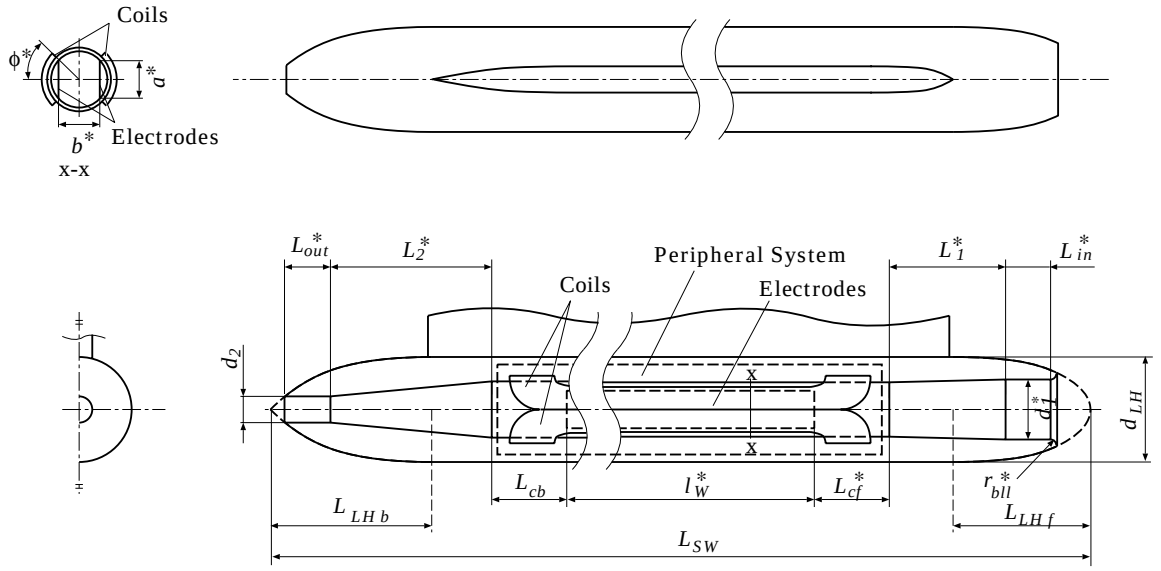

Fig. 7 Inner ducting type thruster and hull

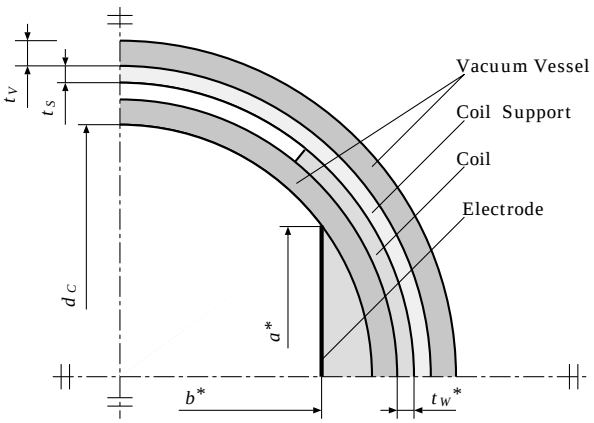

Fig. 8 Section plan of inner ducting type thruster

Table 1 Nondimensional design variables (Inner ducting type)

d_1	=	$\xi_1\bar{d_1}$	L_{out}	=	$\xi_6\bar{L}_{out}$	ϕ	=	$\xi_{11}\bar{\phi}$
r_{b11}	=	$\xi_2\bar{r}_{b11}$	L_1	=	$\xi_7\bar{L}_1$	t_w	=	$\xi_{12}\bar{t}_w$
a	=	$\xi_3\bar{a}$	L_{ef}	=	$\xi_8\bar{L}_2$	I_{cl}	=	$\xi_{13}\bar{I}_{cl}$
b	=	$\xi_4\bar{b}$	L_{ef}	=	$\xi_9\bar{L}_{ef}$			
L_{in}	=	$\xi_5\bar{L}_{in}$	l_W	=	$\xi_{10}\bar{l}_W$			

$\bar{d_1}$, $\bar{r}_{b11}$, ... : the initial dimensions

4.2 Formulation of the optimal design problem

4.2.1 Design variables — Configurations and dimensions of the hull form and thruster systems

(1) The inner ducting type Figures 7 and 8 illustrate the configuration of the SWATH hulls, and the details of the inner ducting type thruster systems. In Figs. 7 and 8, the geometrical dimensions with * mark correspond to the design variables which will be determined by the optimization calculation. As shown in Fig. 7, an inner duct is led through the lower hull in which the MHD thruster is installed. The ductings have a round type section, which are composed of a straight part, a nozzle, and a bellmouth type inlet. The detail section of the MHD thruster is illustrated by Fig. 8. The electrodes are installed in parallel at the midpart of the duct. The superconducting coils with a saddle type shape are installed at both sides in the duct, which are cooled with liquid helium insulated with vacuum vessels.

The design variables are summarized in Table 1, which correspond to the geometrical dimensions with * mark shown in Figs. 7 and 8.

(2) The annular ducting type Figures 9 and 10 illustrate the configuration of the SWATH hulls and the details of the annular type thruster systems. In Figs. 9 and 10, the geometrical dimensions with * mark correspond to the design variables which will be determined by the optimization calculation. As shown in Fig. 9, an annular MHD thruster ring is installed around the hull. This design was referenced to that of Swallom et al. [SWALLOM 1991]. Sea water is accelerated by the

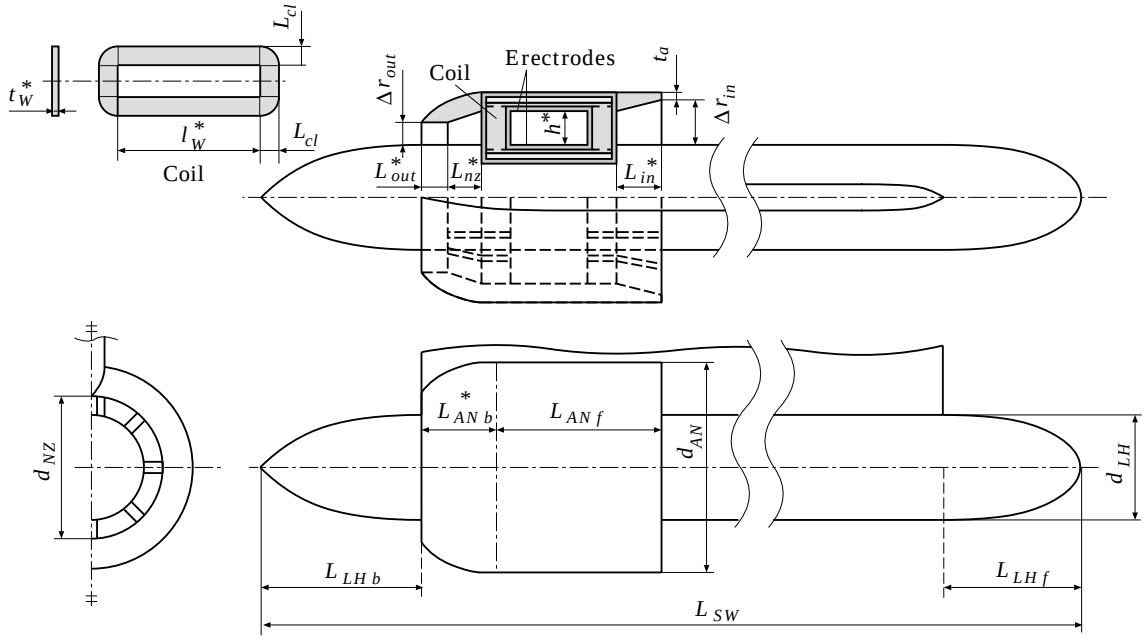

Fig. 9 Annular ducting type thruster and hull

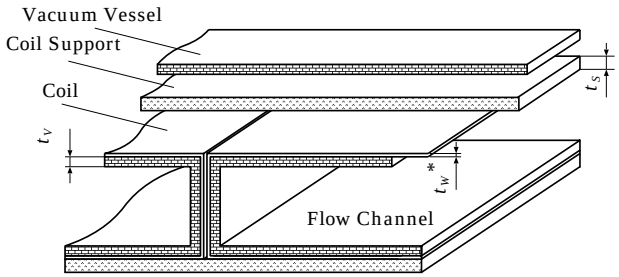

Fig. 10 Section of annular ducting type thruster

electromagnetic field generated in the annular spaces composed of the ring magnets and the ship's hull. The detail section of the thruster is shown in Fig. 10. The superconducting coils form a saddle type shape with double knuckles. The 16-elements of coils are arranged in a circle, which compose the superconducting magnets. The electrodes are installed with a distance of h, which generate the electromagnetic field together with the superconducting magnets.

The design variables are summarized in Table 2, which correspond to the geometrical dimensions with * mark shown in Figs. 9 and 10.

(3) Pod mount type Figures 11 and 12 illustrate the configuration of the SWATH hulls and the details of the pod mount type thruster systems. In Figs. 11 and 12, the dimensions with * mark correspond to the design variables

Table 2 Nondimensional design variables (Annular ducting type

L_1	$= \xi_1\bar{L}_1$	h	$= \xi_4\bar{h}$	l_W	$= \xi_7\bar{l}_W$
L_2	$= \xi_2\bar{L}_2$	L_{ANb}	$= \xi_5\bar{L}_{ANb}$	I_{cl}	$= \xi_8\bar{I}_{cl}$
L_3	$= \xi_3\bar{L}_3$	t_w	$= \xi_6\bar{t}_w$		

$\bar{L}_1$, $\bar{L}_2$, ... : the initial dimensions

Table 3 Nondimensional design variables (Pod mount type)

d_1	$= \xi_1\bar{d}_1$	L_2	$= \xi_8\bar{L}_2$	$\Delta\gamma_p$	$= \Delta\bar{\gamma}_p$
r_{b11}	$= \xi_2\bar{r}_{b11}$	L_{cf}	$= \xi_9\bar{L}_{cf}$	L_{pf}	$= \xi_{16}\bar{L}_{pf}$
a	$= \xi_3\bar{a}$	L_{cb}	$= \xi_{10}\bar{L}_{cb}$	L_{pb}	$= \xi_{17}\bar{L}_{pb}$
b	$= \xi_4\bar{b}$	l_W	$= \xi_{11}\bar{l}_W$	r_{pc}	$= \xi_{18}\bar{r}_{pc}$
L_{in}	$= \xi_5\bar{L}_{in}$	ϕ	$= \xi_{12}\bar{\phi}$	L_{pt}	$= \xi_{19}\bar{L}_{pt}$
L_{out}	$= \xi_6\bar{L}_{out}$	T_w	$= \xi_{13}\bar{t}_w$	θ	$= \xi_{20}\bar{\theta}$
L_1	$= \xi_7\bar{L}_1$	I_{cl}	$= \xi_{14}\bar{I}_{cl}$		

$\bar{d}_1$, $\bar{r}_{b11}$, ... : the initial dimensions

which will be determined by the optimization calculation. The shape of the thruster surface is defined as a spheroidal form in the forepart and as a parabolic – revolution form in the aftpart together with a parallel form in the midpart.

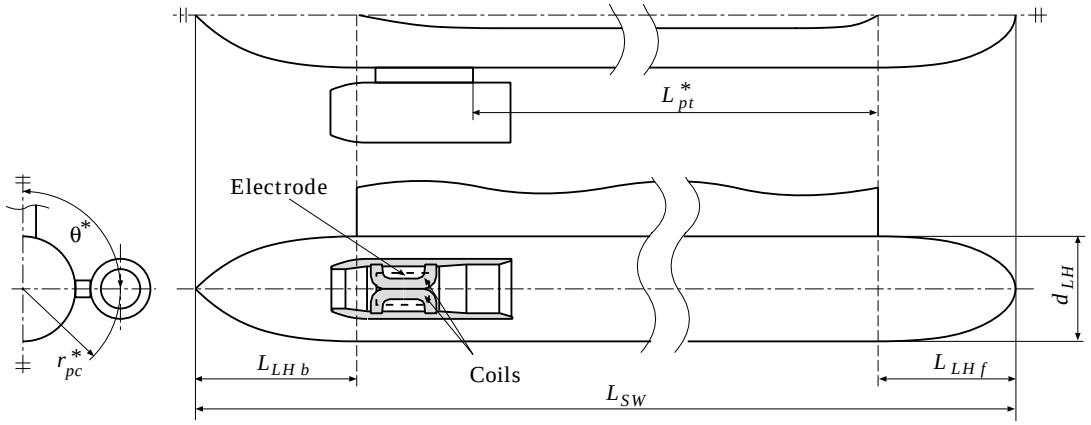

Fig. 11 Pod mount type thruster and hull

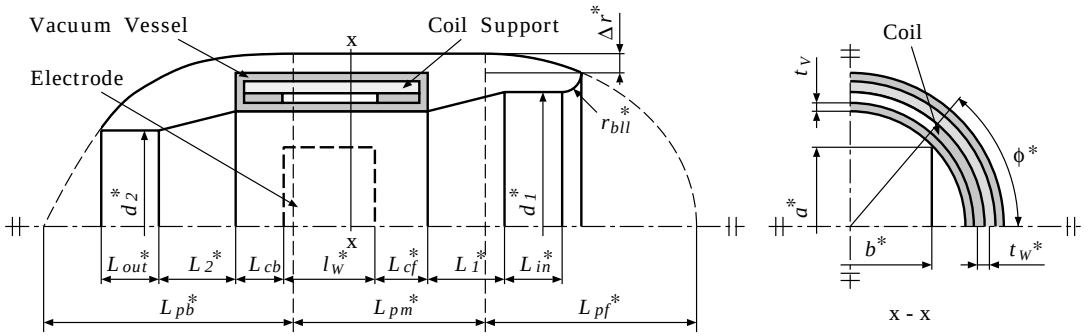

Fig. 12 Detail of pod mount type thruster

The configuration is similar to the inner ducting type as mentioned in item (1).

The design variables are summarized in Table 3, which correspond to the geometrical dimensions with * mark shown in Figs. 11 and 12.

4.2.2 Design conditions and constraints

The design conditions and constraints, which are common to each type of thruster systems, are provided as follows.

Ship speed The ship speed is assumed to be constant (U = 20 knots) for each type of systems during optimization.

Displacement The displacement is assumed to be the same value within the allowance for each type of systems.

Center of buoyancy Removal of C.B. is limited within the allowance.

Residual displacement The displacement after reducing the weight of the superconducting coils and their holding devices is assumed to be not less than 100 tons.

Critical condition of the superconducting coil The critical condition of superconducting current I_{cl} is determined based on the today's technical level [SHIMAMOTO 1991].

$$I_{cl} \leq I_{max} \tag{27}$$

where, I_{max} is the upper limit of the current, which is taken as 183.2A for NbTi wire. Based on the value of I_{cl}, the current density J_{cl} of the superconducting current in equation (12) can be expressed as,

$$J_{cl} = \frac{nI_{cl}}{h_{cl}W_{cl}} \tag{28}$$

where, n : number of coil loops in the coil tape (= 25), h_{cl} : height of the coil tape (= 10.86 mm), W_{cl} : mean width of the coil tape (= 1.77 mm).

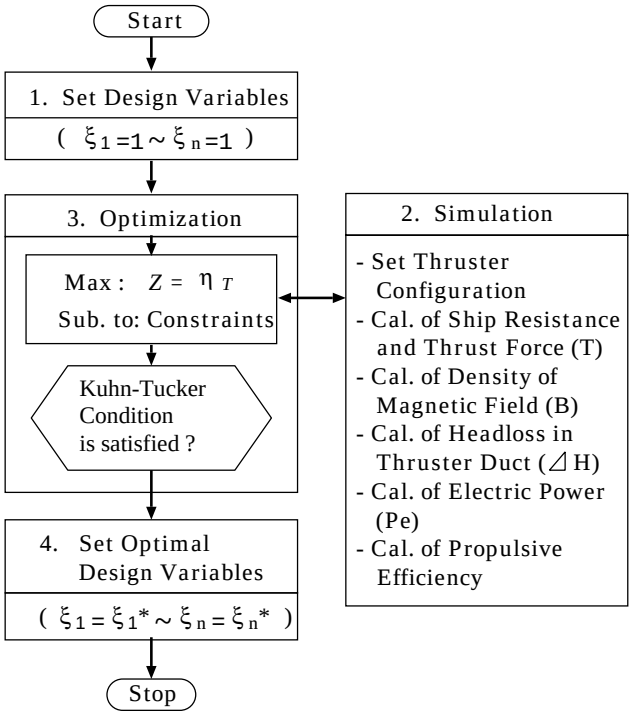

Fig. 13 Solution procedure of optimization problem

Volume of coils The volume of the superconducting coils is assumed to be of the same value for each type of the systems.

The individual constraints for each type of thruster systems are given by the formula of the resistance of the ship, the hydraulic drag relations of the ductings, the electromagnetic performance of the MHD thrusters etc. which were mentioned in chapter 3. The geometric relations of the hull and the thruster shown in Figs. 7 $\sim$ 12 are also taken as the constraints for the optimization.

4.2.3 Objective function

The objective function Z for each type of the thruster systems is taken as maximizing the overall propulsive efficiency η_T given by equation (14). Namely,

$$\text{Maximize} : Z = \eta_T \tag{29}$$

4.3 Solution procedure of the optimization problems

The above optimization problems include various nonlinear functions and complex calculations of the performance of the ship and the thrusters, which are formulated as a kind of nonlinear optimization problem. Figure 13 indicates the solving algorithm of the problem which is composed of the simulation calculation of the performance and the optimization procedure. The simulation calculating the performance is coupled with the optimization procedure and repeated in every steps. For the searching algorithm of the optimization calculation, a Generalized Reduced Gradient (GRG) method was adopted together with examining satisfaction of the Kuhn-Tucker condition.

Table 4 Principal dimensions of the ship

L_{SW}	24.0 m	L_{ST}	17.0 m
L_{LHf}	4.0 m	L_{STf}	12.0 m
L_{LHb}	3.0 m	L_{STb}	4.0 m
d_{LH}	2.0 m	W_{ST}	0.7 m
y_l	12.0 m	h_{ST}	1.0 m

5 Results of Optimization and Evaluation of Each Thruster System

In this chapter, the results of the optimization is presented, and the propulsive efficiency of each thruster system is compared and evaluated together with its advantage and disadvantage.

5.1 Given numerical condition of the optimization

The calculating model is assumed to be the design of an experimented SWATH ship with the displacement of about 180 tons, the length of 24 m and the speed of 20 knots (Froude number $= 0.67$). The principal dimensions of the ship is listed in Table 4. The volume of superconducting coils is assumed to be 1.0 m^3. The side constraints for design variables are set as,

$$0.5 \leq \xi_i \leq 1.5 \tag{30}$$

5.2 Results of optimization

The results of the optimization for each thruster system are as follows.

(1) Inner ducting type Table 5 shows the initial and the optimized geometrical dimensions of the thruster system. In the table, some design variables show the values of interior optima, while the others are bounded to the side constraints. The length of the electrode l_W is bounded to the value of the upper constraint ($\xi_{10} = 1.5$). The discussion and evaluation will be

Table 5 Results of optimization for inner ducting system

(a) Initial dimensions			
d_1	1.0 m	L_2	4.5 m
r_{bll}	7.5 cm	L_{cf}	1.5 m
a	0.5 m	l_W	6.5 m
b	0.6 m	ϕ	60 deg
L_{in}	2.0 m	t_W	3.0 cm
L_{out}	1.5 m	J	150 A
L_1	3.5 m		

(b) Optimized dimensions			
$\xi_1{}^*(d_1)$	1.265897	$\xi_8{}^*(L_2)$	0.772327
$\xi_2{}^*(r_{bll})$	1.500000	$\xi_9{}^*(L_{cf})$	0.657462
$\xi_3{}^*(a)$	1.128945	$\xi_{10}{}^*(l_W)$	1.500000
$\xi_4{}^*(b)$	1.417948	$\xi_{11}{}^*(\phi)$	1.003352
$\xi_5{}^*(L_{in})$	0.553163	$\xi_{12}{}^*(t_W)$	1.183329
$\xi_6{}^*(L_{out})$	0.500000	$\xi_{13}{}^*(J)$	1.190426
$\xi_7{}^*(L_1)$	1.500000	η_T	0.057872

Table 6 Results of optimization for the annular ducting system

(a) Initial dimensions			
L_{in}	0.5 m	L_{ANb}	1.5 m
L_{nz}	0.5 m	t_W	2.0 cm
L_{out}	1.0 m	l_W	3.0 m
h	0.5 m	J	150 A

(b) Optimized dimensions			
$\xi_1{}^*(L_{in})$	1.160378	$\xi_5{}^*(L_{ANb})$	0.500000
$\xi_2{}^*(L_{nz})$	0.500000	$\xi_6{}^*(t_W)$	1.124994
$\xi_3{}^*(L_{out})$	0.500000	$\xi_7{}^*(l_W)$	0.897285
$\xi_4{}^*(h)$	1.098544	$\xi_8{}^*(J)$	1.221333
		η_T	0.032144

summarized in later section with the results for other two cases.

(2) Annular ducting type Table 6 shows the initial and the optimized geometrical dimensions of the thruster system. Some design variables show the values of interior optima, while the other variables are bounded to the side constraints. The length of the outlet duct becomes shorter after optimized, which means that the headloss in the duct is minimized.

Table 7 Results of optimization for the pod mount system

(a) Initial dimensions			
d_1	1.0 m	l_W	2.5 m
r_{bll}	0.1 m	ϕ	60 deg
a	0.6 m	t_W	3.0 cm
b	0.6 m	J	150 A
L_{in}	0.25 m	Δr	0.2 m
L_{out}	0.25 m	L_{pf}	2.0 m
L_1	0.45 m	L_{pb}	2.0 m
L_2	0.45 m	r_{pc}	2.0 m
L_{cf}	1.0 m	L_{pt}	12.0 m
L_{cb}	1.0 m	θ	90 deg

(b) Optimized dimensions			
$\xi_1{}^*(d_1)$	1.218687	$\xi_{11}{}^*(l_W)$	1.500000
$\xi_2{}^*(r_{bll})$	1.500000	$\xi_{12}{}^*(\phi)$	1.045827
$\xi_3{}^*(a)$	0.965164	$\xi_{13}{}^*(t_W)$	1.144667
$\xi_4{}^*(b)$	1.464322	$\xi_{14}{}^*(J)$	1.221333
$\xi_5{}^*(L_{in})$	0.912083	$\xi_{15}{}^*(\Delta r)$	0.500000
$\xi_6{}^*(L_{out})$	0.856960	$\xi_{16}{}^*(L_{pf})$	1.304242
$\xi_7{}^*(L_1)$	1.256391	$\xi_{17}{}^*(L_{pb})$	1.445834
$\xi_8{}^*(L_2)$	0.841800	$\xi_{18}{}^*(r_{pc})$	1.004672
$\xi_9{}^*(L_{cf})$	1.008935	$\xi_{19}{}^*(L_{pt})$	1.056209
$\xi_{10}{}^*(L_{cb})$	1.008935	$\xi_{20}{}^*(\theta)$	1.419170
		η_T	0.043742

(3) Pod mount type Table 7 shows the initial and the optimized geometrical dimensions of the thruster system. Most of the design variables shows the interior optima, while the few variables are bounded to the side constraints. The length of the electrode l_W is bounded to the value of the upper constraint ($\xi_{11} = 1.5$).

5.3 Comparison and evaluation of each type thruster system

Based on the results shown in Tables 5 $\sim$ 7 the optimized shapes of the hull and the thrusters for respective configurations of the inner ducting, the annular ducting and the pod mount type are shown in Figs. 14 $\sim$ 16. In the figures, they are also compared with the initial shapes.

Through the all three types of the thruster systems, the hull forms have changed their shapes so as to reduce the resistance. And, the MHD channels of the thrusters have

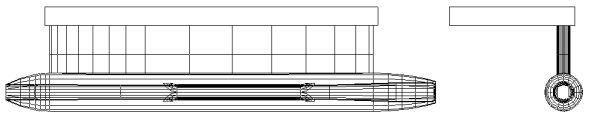

(a) Initial configuration

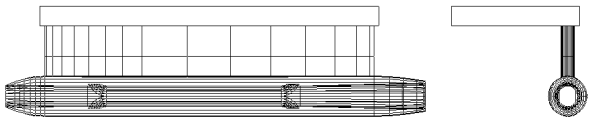

(b) Optimized configuration

Fig. 14 Optimized shapes of the hull and the thruster for inner ducting system

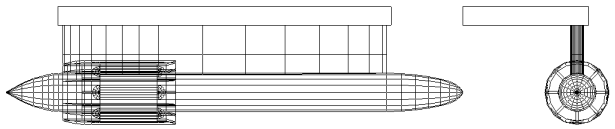

(a) Initial configuration

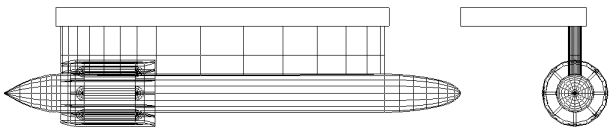

(b) Optimized configuration

Fig. 15 Optimized shapes of the hull and the thruster for annular ducting system

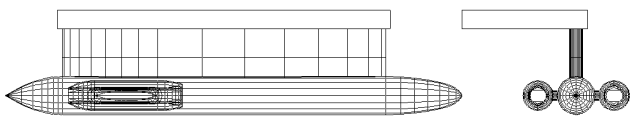

(a) Initial configuration

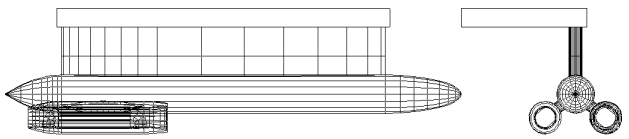

(b) Optimized configuration

Fig. 16 Optimized shapes of the hull and the thruster for pod mount system

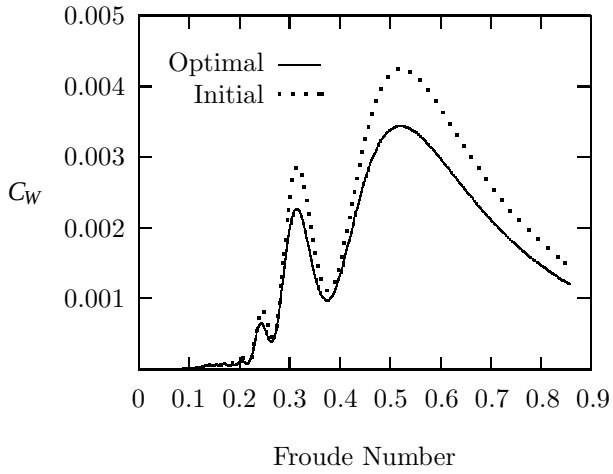

Fig. 17 Coeff. of wave-making resistance (Inner ducting system)

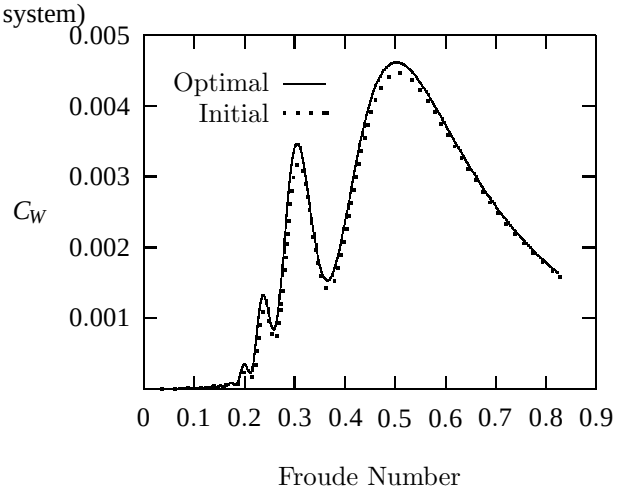

Fig. 18 Coeff. of wave-making resistance (Annular ducting system)

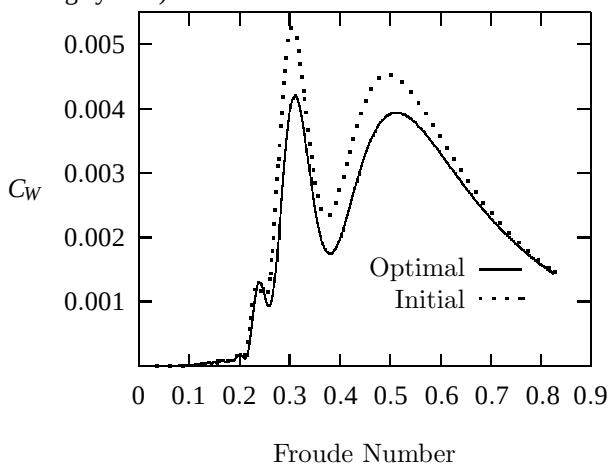

Fig. 19 Coeff. of wave-making resistance (Pod mount system)

been enlarged up to the upper limit which is bounded to the constraints as mentioned before. In the case of the annular ducting and the pod mount type thrusters, the positions of the thruster have moved from the initial positions to the aft and lower positions after optimization.

Figures 17 $\sim$ 19 illustrate the curves of the wave-making resistance which were calculated during the optimization procedure. The Froude number was increased up to 0.85. According to Figs. 17 $\sim$ 19, the wave-making resistance indicates the lowest value in the case of the inner ducting type, while the annular ducting type indicates the highest value. The figures also indicate the comparison between

Table 8 Comparison of optimized results among three types of systems

	Inner ducting	Annular ducting	Pod mount
Displacement (ton)	180.000	177.571	192.715
Froude No.	0.69109	0.66380	0.66380
Ship resistance (kN)	101.442	113.931	133.920
Flow rate in duct (m^3/s)	12.9496	49.1956	12.0017
Headloss in duct (maq)	9.08938	2.98614	5.12522
Density of magnetic field (T)	8.61197	5.92690	5.54785
Electric power (MW)	9.01758	36.4682	31.5004
Hydraulic efficiency (%)	44.1086	39.6917	55.7128
Electrical efficiency (%)	13.1203	8.09834	7.85133
Propulsive efficiency (%)	5.78718	3.21437	4.37420

Table 9 Results for $I_{max} = 200$A (Artificial condition)

	Inner ducting	Annular ducting	Pod mount
Displacement (ton)	137.165	201.272	187.079
Froude No.	0.68296	0.66380	0.66380
Ship resistance (kN)	79.4967	115.074	126.985
Flow rate in duct (m^3/s)	4.74659	57.5368	6.75501
Headloss in duct (maq)	17.9048	3.91511	8.83768
Density of magnetic field (T)	17.7398	7.82446	18.4579
Electric power (MW)	6.36749	18.3538	6.97988
Hydraulic efficiency (%)	47.8732	29.8980	54.4317
Electrical efficiency (%)	39.4655	21.5762	34.3891
Propulsive efficiency (%)	18.8932	6.45087	18.7186

the initial and the optimized value of the wave-making resistance for each type of thrusters. In the case of the inner ducting and the pod mount type, the resistance performance is fairly improved by the optimization calculations, while it is slightly improved for the annular ducting type. These results would be caused by the effect of wave interference among the strut, the lower hull and the thruster.

Table 8 shows the results of the optimized propulsive efficiency and their comparison among three thruster systems. According to the results, the inner ducting type thruster indicates the highest propulsive efficiency among three types, while the annular ducting type indicates the lowest efficiency.

The above reason is as follows. In the case of the inner ducting type thruster, a large volume of the electromagnetic field can be given although the long hydraulic duct (namely, higher hydraulic drag) is required; which results in higher propulsive efficiency. On the contrary, in the case of the annular ducting type, the volume of the electromagnetic field is very limited, which consequently increases the electric power. The pod mount system has a short hydraulic duct which causes lower drag and higher hydraulic efficiency. However, it also causes reducing the volume of the electromagnetic field, and consequently electrical efficiency becomes lower. And, the overall propulsive efficiency given by the product of the above two terms is ranked between the former two systems.

In general, it is found that the propulsive efficiency of the MHD thruster is very low compared with the conventional propulsive system. The reason is due to low electrical conductivity of sea water as mentioned in section 3.4. In order to improve the propulsive efficiency, it is necessary

to increase the density of the electromagnetic field, which has been limited by the today's level of the superconducting technology being based on using NbTi material.

Finally, we examine how the propulsive efficiency could be increased, if superconducting material were improved. This is tried by applying a simulation in which the constraint of I_{max} in equation (27) is artificially increased up to $I_{max} = 200$A. The result is shown in Table 9. According to this result, the propulsive efficiency is improved up to ab. 20 %, and then the density of B in the thruster becomes up to ab. 20 T. This result would be hopeful. However, this improvement depends on the future technology of superconductivity.

6 Concluding Remarks

Optimal design of the superconducting MHD thruster system was investigated. Three kinds of configurations of the systems, namely the inner ducting type, the annular ducting type and the pod mount type thrusters, were designed to install in an experimental ship with SWATH hulls. After that, the optimal designs were examined and evaluated for each type of thruster systems. According to the results of the optimization calculations, the inner ducting type shows the highest propulsive efficiency. The annular ducting type shows the lowest efficiency due to the space limitation of the superconducting magnet. The pod type is ranked between these two. Although the optimal design was adopted, the propulsive efficiency of the MHD thruster system still remained in very low level compared with the conventional propulsion system, which was caused by low electrical conductivity of sea water. In order to improve the efficiency, the level-up of the superconducting technology including the improvement of coil material is urged.

Acknowledgement

The authors wish to express their thanks to Dr. Shimamoto, former chief engineer of the Kobe shipyard, Mitsubishi Heavy Industries Ltd., who helped them with referring to his experience of the study on the experimental superconducting MHD ship "YAMATO-1".

References

[CHAPMAN 1972] Chapman, R. B., (1972), "Hydrodynamic Drag of Semisubmerged Ships", *Trans. ASME, J. of Basic Eng.*, Vol. 94, pp. 879-884.

[DORAGH 1963] Doragh, L. R. A., (1963), "Magneto-hydrodynamic Ship Propulsion Using Superconducting Magnets", *Trans. SNAME*, 71, pp. 370-386.

[MOTORA 1991] Motora, S. et al., (1991), "An Outline of the R&D Project on Superconducting MHD Ship Propulsion in Japan", *Proc. MHD 91*, Paper 1-1.

[PAPANIKOLAOU 1991] Papanikolaou, A. and Androulakakis, M., (1991), "Hydrodynamic Optimization of High-Speed SWATH", *Proc. of FAST 91*, Vol. 1, pp. 507-521.

[RICE 1961] Rice, W. A., (1961), *U.S. Patent, 2997013*.

[SALVESEN 1985] Salvesen, N. et al., (1985), "Hydro-Numeric Design of SWATH ships", *Trans. SNAME*, 93, pp. 325-346.

[SHIMAMOTO 1991] Shimamoto, K. et al., (1991), "Design, Manufacturing and Characteristics of Superconducting Magnet for YAMATO-1", *Proc. MHD 91*, pp. 2-1-1∼2-1-5.

[SWALLOM 1991] Swallom, D. W. et al., (1991), "Magneto-hydrodynamic Submarine Propulsion Systems", *Naval Engineering J.*, May 1991, pp. 141-157.

[WAY 1967] Way, S. and Devlin, C., (1967)," Prospects for the Electromagnetic Submarine", *AIAA Paper* 67-432.